The Role of Intraseasonal Variability in the Nature of Asian Monsoon Precipitation

CARLOS D. HOYOS AND PETER J. WEBSTER

School of Earth and Atmospheric Sciences, Georgia Institute of Technology, Atlanta, Georgia

(Manuscript received 8 December 2005, in final form 25 January 2007)

ABSTRACT

The structure of the mean precipitation of the south Asian monsoon is spatially complex. Embedded in a broad precipitation maximum extending eastward from 70°E to the northwest tropical Pacific Ocean are strong local maxima to the west of the Western Ghats mountain range of India, in Cambodia extending into the eastern China Sea, and over the eastern tropical Indian Ocean and the Bay of Bengal (BoB), where the strongest large-scale global maximum in precipitation is located. In general, the maximum precipitation occurs over the oceans and not over the land regions. Distinct temporal variability also exists with time scales ranging from days to decades. Neither the spatial nor temporal variability of the monsoon can be explained simply as the response to the cross-equatorial pressure gradient force between the continental regions of Asia and the oceans of the Southern Hemisphere, as suggested in classical descriptions of the monsoon. Monthly (1979–2005) and daily (1997–present) rainfall estimates from the Global Precipitation Climatology Project (GPCP), 3-hourly (1998–present) rainfall estimates from the Tropical Rainfall Measuring Mission (TRMM) microwave imager (TMI) estimates of sea surface temperature (SST), reanalysis products, and satellite-determined outgoing longwave radiation (OLR) data were used as the basis of a detailed diagnostic study to explore the physical basis of the spatial and temporal nature of monsoon precipitation.

Propagation characteristics of the monsoon intraseasonal oscillations (MISOs) and biweekly signals from the South China Sea, coupled with local and regional effects of orography and land–atmosphere feedbacks are found to modulate and determine the locations of the mean precipitation patterns. Long-term variability is found to be associated with remote climate forcing from phenomena such as El Niño–Southern Oscillation (ENSO), but with an impact that changes interdecadally, producing incoherent responses of regional rainfall. A proportion of the interannual modulation of monsoon rainfall is found to be the direct result of the cumulative effect of rainfall variability on intraseasonal (25–80 day) time scales over the Indian Ocean. MISOs are shown to be the main modulator of weather events and encompass most synoptic activity.

Composite analysis shows that the cyclonic system associated with the northward propagation of a MISO event from the equatorial Indian Ocean tends to drive moist air toward the Burma mountain range and, in so doing, enhances rainfall considerably in the northeast corner of the bay, explaining much of the observed summer maximum oriented parallel to the mountains. Similar interplay occurs to the west of the Ghats. While orography does not seem to play a defining role in MISO evolution in any part of the basin, it directly influences the cumulative MISO-associated rainfall, thus defining the observed mean seasonal pattern. This is an important conclusion since it suggests that in order for the climate models to reproduce the observed seasonal monsoon rainfall structure, MISO activity needs to be well simulated and sharp mountain ranges well represented.

1. Introduction

A fundamental requirement for agricultural development and water resource management in the south and Southeast Asian region is a better predictive capability of internal and external variability of summer monsoon rainfall on time scales ranging from weeks to several years (e.g., Parthasarathy et al. 1988; Webster et al. 1998; Lal et al. 1999; Gadgil et al. 1999, 2002). As the Asian summer monsoon is a major component of global climate dynamics, it has the potential of imparting variability on the climates of other components (e.g., Webster and Yang 1992; Webster et al. 1998; Kirtman and Shukla 2000). Therefore, improvements in the predictability of the monsoon will lead to increased predictability elsewhere. The fundamental hypothesis of this study is that a greater understanding of the physical

Corresponding author address: Carlos D. Hoyos, Georgia Institute of Technology, 311 Ferst Dr., Atlanta, GA 30332.
E-mail: choyos@eas.gatech.edu

DOI: 10.1175/JCLI4252.1

processes determining the mean seasonal monsoonal precipitation patterns will lead to better predictions and provide milestones for numerical climate modeling.

There is little disagreement on the fundamental mechanism that drives monsoon circulations. Essentially, this is a cross-equatorial pressure gradient formed by the differential heating between the landmasses of the summer hemisphere and the oceans of the winter hemisphere. However, the spatial and temporal variability of monsoon precipitation is far more complicated than that which can be expected from such a slowly varying cross-equatorial pressure gradient. In fact, the processes that produce the specific spatial distribution of even the long-term mean precipitation are not clearly understood. Different processes, phenomena, and geographic features have been suggested as modulators of monsoon precipitation, such as local and regional effects of orography (e.g., Grossman and Garcia 1990; Grossman and Durran 1984; Xie et al. 2006), propagation characteristics of the monsoon intraseasonal oscillation (MISO) that involve both the ocean and the atmosphere (e.g., Lawrence and Webster 2002; Jiang et al. 2004; Wang et al. 2005), propagation of biweekly signals from the South China Sea (Annamalai and Slingo 2001), and land–atmosphere feedback (e.g., Webster 1983). All of these features of the monsoon in isolation or in combination appear as possible candidates.

This paper is an attempt to determine the mechanisms responsible for the variability and structure of summer monsoon rainfall on different time scales and regions within Asia. Figure 1 provides a geographical reference for the regions discussed in the text. These regions include the east Indian Ocean (EIO), Bay of Bengal (BoB), central India (CI), Gangetic Plains (GP), Western Ghats (WG), and Cambodia (CMD). These areas were selected based on geography and seasonal average precipitation: BoB, WG, and CMD correspond to regional rainfall maxima associated with the summer monsoon, EIO is a key region in order to understand different features of the MISO, CI is an area over land that is strongly modulated by the MISO, and GP corresponds to a very important geomorphologic and hydrographic unit, vital for the development of India and Bangladesh, whose precipitation is determined by the Southeast Asian monsoon and its variability.

Figure 2a shows the spatial distribution of the mean cumulative rainfall from June to September (JJAS) over the period 1979–2004 using the Global Precipitation Climatology Project (GPCP) data discussed in the next section, as well as the mean annual cycle of rainfall over the six regions previously described (Fig. 2b). It is

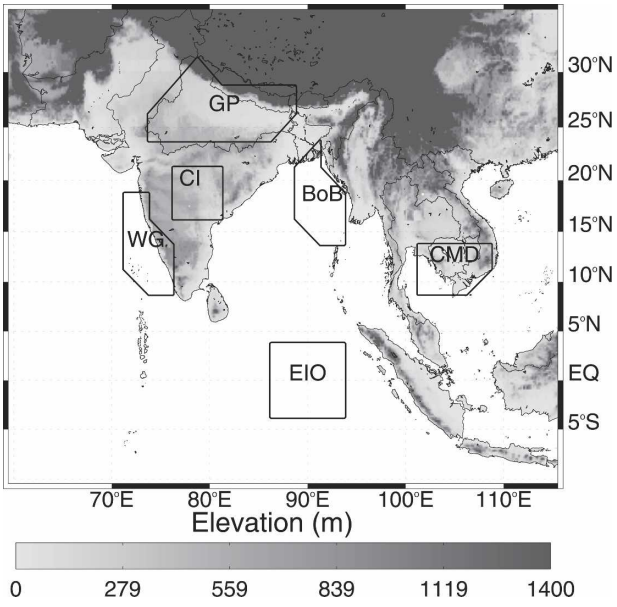

FIG. 1. Geographical reference for the regions discussed in the text and elevations (shading).

evident from Fig. 2a that there is a complex spatial pattern of rainfall associated with the Asian monsoon system, with localized precipitation maxima to the west of the WG foothills in India with a total of 850 mm during JJAS, to the east side of the BoB with 1430 mm, and over CMD with 1050 mm. While the overall driving mechanism of the monsoon is the slowly varying cross-equatorial pressure gradient force, the rainfall is strongly regional with maxima occurring over the ocean regions and neither over the Asian continent nor the Indian subcontinent as initially noted by Grossman and Garcia (1990). In fact, the BoB possesses the largest global maximum of boreal summer rainfall on the planet. It is interesting to note that total summer precipitation drops almost linearly between the Bay of Bengal (>1200 mm), across central India (800 mm), and into Pakistan (200–300 mm).

The rainfall maximum over the EIO (860 mm) does not have a monsoonlike annual cycle and is relatively constant throughout the year (Fig. 2b). However, it has been shown to be intimately related to monsoonal intraseasonal variability (e.g., Webster et al. 1998; Lawrence and Webster 2002). In contrast to the near-equatorial precipitation, summer rainfall farther north and east over the Bay of Bengal and Southeast Asian countries commences in May. Over most of continental India, however, rainfall starts later during June (Fig. 2b). In fact, a number of studies consider the EIO as the source region of monsoon intraseasonal variability that possesses the largest amplitude of all monsoon precipi-

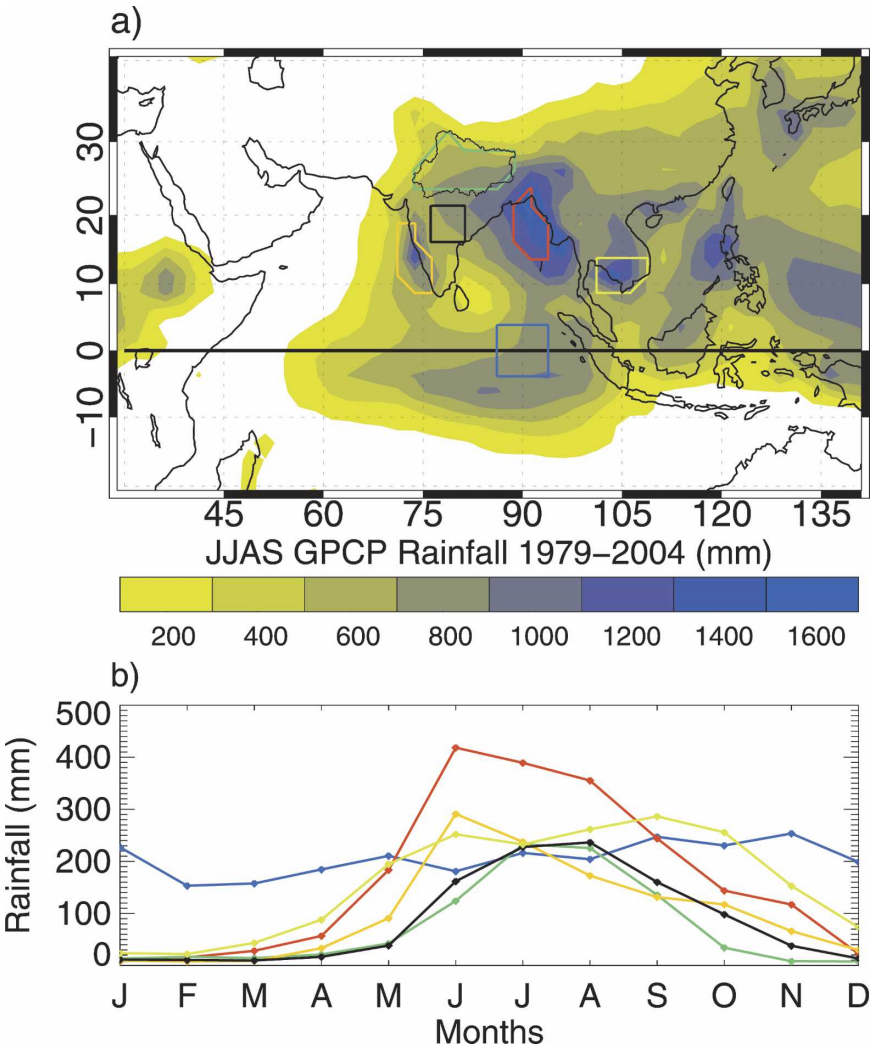

FIG. 2. (a) Mean south and Southeast Asian summer monsoon rainfall (JJAS) averaged from 1979 to 2004 using the monthly GPCP data and (b) mean annual cycle of rainfall over the six regions outlined in Fig. 1. The lines in color correspond to the colors in (a).

tation variations (e.g., Webster et al. 1998; Lawrence and Webster 2002; Waliser et al. 2003a,b) producing active and break periods of the south Asian monsoon on 25–80-day time scales.

In the BoB, precipitation occurs as a maximum parallel to the Burma mountains (Fig. 2a) as noted by Grossman and Garcia (1990) and Xie et al. (2006). But what are the main processes that determine the rainfall maximum? Is the maximum produced by the mean onshore flow from the basic southwesterlies of the monsoon producing rainfall through orographic uplift? Does the freshness and warmth of the bay itself play any role so that if there were no Burmese Mountains there would still be a regional precipitation maximum? Furthermore, for whatever reason there is a maximum in the BoB, what time scales of motion contribute to its existence? Zuidema (2003), Grossman and Garcia (1990), and Xie et al. (2006) examined this question but the first study considered only two summers while the latter two used monthly data. Thus it is difficult to determine the relative role of intraseasonal variability or synoptic events, for example, in producing the maximum. Indian monsoon rainfall precipitation has proven to be very difficult to model, which is evident from the results of the Atmospheric Model Intercomparison project as summarized by Gadgil and Sanjani (1998) and Sperber and Palmer (1996). In fact, simulation of mean monsoon precipitation in general has been elusive in models. It is important to determine whether or not these failures result because of the poor represen-

TABLE 1. JJAS rainfall correlations among different regions for the period 1979–2004.

	EIO	BoB	CI	GP	WG	CMD	AIRI
EIO	1.00						
BoB	−0.24	1.00					
CI	0.10	−0.37	1.00				
GP	−0.21	0.32	0.35	1.00			
WG	0.18	−0.06	0.59	0.13	1.00		
CMD	0.04	0.45	0.05	0.42	0.32	1.00	
AIRI*	−0.16	0.06	0.60	0.56	0.48	0.28	1.00

* Data obtained from the Indian Institute of Tropical Meteorology (see online at www.tropmet.res.in) positive correlations greater than 0.39 (0.50) are significant at a 95% (99%) level.

tation of orography, for example, or the general absence in many numerical models of specific phenomena such as intraseasonal variability.

The complexity of the summer monsoon rainfall is not restricted to spatial patterns but also to its variation in time. The monsoon possesses a strong temporal variability ranging from the diurnal, to the synoptic and intraseasonal, and then to interannual time scales. In fact, this complicated structure extends to the relationship between interannual variability of each of the monsoon regions we consider. These interregional correlations are summarized in Table 1 for the period 1979–2004. It is important to note that scatterplots (not shown here) do not show the presence of extreme outliers modifying the correlations artificially. The complexity may be seen by comparing the interannual correlations between the BoB, CI, and GP, which we may expect to be highly correlated. The JJAS seasonal rainfall correlation between the BoB and the GP is 0.37, which is higher and of the opposite sign to that between the BoB and CI (−0.32). The reason for this dissimilarity in magnitude and sign between the correlations is unclear. Furthermore, why is the correlation between the BoB and CMD larger than between the BoB and the GP? Why is the precipitation in EIO so poorly correlated with all of the monsoon regions? The All-India Rainfall Index (AIRI; Parthasarathy et al. 1987) correlates well with CI, moderately with GP and WG, but very weakly with BoB. Are the relative weaknesses of the correlations or even their absence between regions indicating that other higher-frequency variability links different parts of the monsoon?

The questions raised above will be addressed in the following diagnostic study. Section 2 describes the datasets used in the study. Section 3 provides an overview of precipitation in south Asia. Sections 4 and 5 describe further analysis and present results of the analysis. Section 6 offers some conclusions.

2. Data

A number of different datasets are used in the study. These are described briefly below.

a. GPCP products

Monthly and daily rainfall products of the global merged precipitation analysis (GPCP; Huffman et al. 1997, 2001; Adler et al. 2003) are used to study the temporal and spatial rainfall variability of the Southeast Asian monsoon. The monthly precipitation dataset covers a 26-yr period from January 1979 to the present and the daily dataset extends from 1997 to the present. This dataset is available online (see www.gewex.org/gpcp.html).

b. TRMM precipitation product

The 3-hourly Tropical Rainfall Measuring Mission (TRMM product 3B42; Adler et al. 2000) data are used to describe the rainfall patterns within the wet and dry spells associated with monsoon intraseasonal variability. The spatial resolution of this dataset is 0.25° with data from January 1998 to the present. All TRMM datasets are distributed by the Goddard Distributed Active Archive Center (see online at lake.nascom.nasa.gov/data/dataset/TRMM/). The 3-hourly TRMM data are an optimal combination of different high-quality microwave products to adjust infrared estimates from high-frequency geostationary observations (see online at http://trmm.gsfc.nasa.gov/3b42.html). Therefore, the dataset does not have aliasing issues arising from satellite sampling issues and it provides a reasonably good idea of the convective activity within the day. TRMM precipitation radar data (product 2A25) are also used to provide details of the vertical structure of rainfall in one of the cases studied.

c. NCEP–NCAR reanalysis, OLR, and SST

We use daily zonal and meridional wind components obtained from the National Centers for Environmental Prediction–National Center for Atmospheric Research (NCEP–NCAR) reanalysis product (Kalnay et al. 1996), archived on a 2.5° grid, to find the relationship between rainfall distributions and monsoon dynamics. Outgoing longwave radiation (OLR) data from the Climate Diagnostics Center (CDC) interpolated dataset (Liebmann and Smith 1996) are also utilized in addition to the 3-day average 0.25° gridded TRMM microwave imager (TMI) SST data (Wentz 1997). TMI has the advantage over IR data of being able to measure SST in the presence of nonprecipitating clouds (Wentz and Schabel 2000). Reanalysis and OLR data were pro-

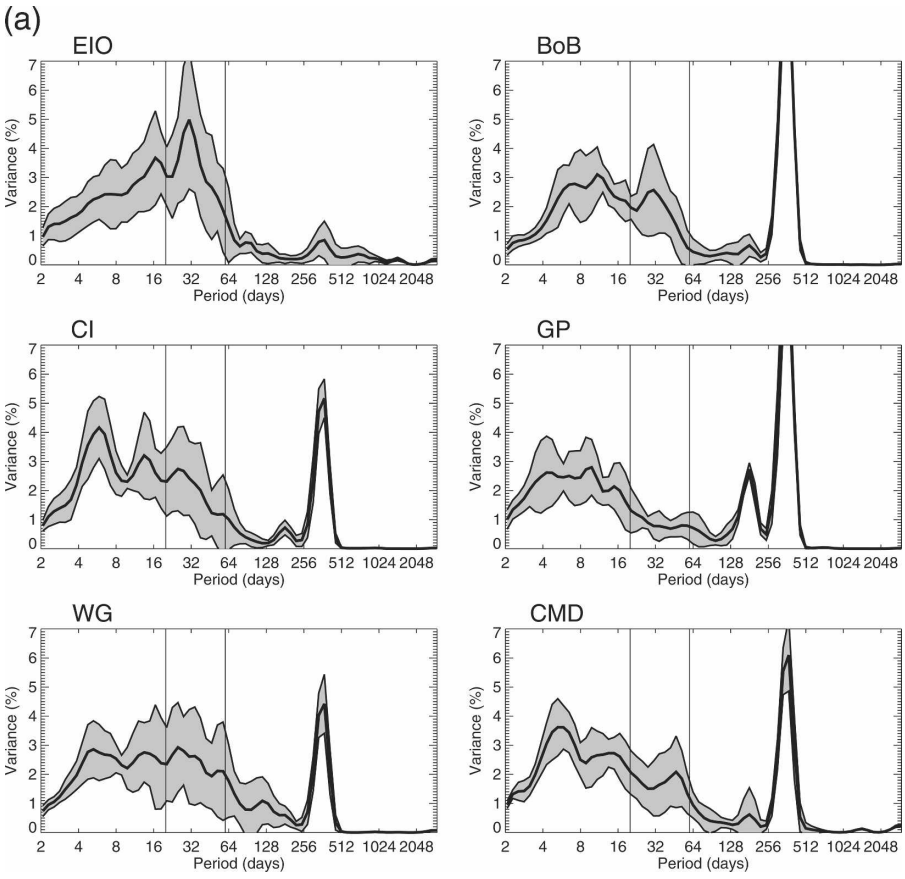

FIG. 3. Summer average wavelet spectra for (a) 1997–2004 daily GPCP rainfall and (b) 1980–2005 daily OLR for each region of Fig. 1. The shaded area represents ±1 standard deviation of the summer spectra.

vided by the Climate Diagnostics Center (see online at www.cdc.noaa.gov). Quick Scatterometer (QuikSCAT) and TMI data are available from the Remote Sensing Systems servers (see online at www.remss.com).

3. Overview of summer monsoon precipitation

Even though the amplitudes of the rainfall maxima shown in Fig. 2a change from year to year, they remain persistent climatological features. However, as suggested by the correlations shown in Table 1, the respective changes in seasonal rainfall from year to year for the different regions do not appear to be interrelated, suggesting strong internal variability in the monsoon system, possibly associated with intraseasonal activity. Different authors have previously pointed out that a proportion of the interannual modulation of the monsoon rainfall is found to be essentially independent of influences external to the Indian Ocean (e.g., Torrence and Webster 1999; Kumar et al. 1999). Large amplitude and large-scale interannual variability is evident in the rainfall anomalies for each JJAS period between 1997 and 2004, relative to the long-term mean (figure not shown). Most often anomalies of different signs lie across different parts of south and Southeast Asia. Over India, the spatial complexity of the patterns calls into question, once again, the usefulness of using the AIRI as a measure of Indian monsoon rainfall variability. Only in 2002 is all of India dominated by an anomaly of the same sign. The identification of high-amplitude internal monsoon variability is very important, as it may obscure signals of the interaction between the monsoon system and other major phenomena of the global climate, such as the ENSO system.

Spectral analysis of daily time series of rainfall reveals the importance of the intraseasonal variability present in monsoon rainfall. Figures 3a,b show the average wavelet spectra for the rainfall and OLR over the six regions obtained using techniques described by Torrence and Compo (1998). The solid line shows the average spectra and the shaded region encloses ±1 standard deviation. Since the wavelet analysis provides time

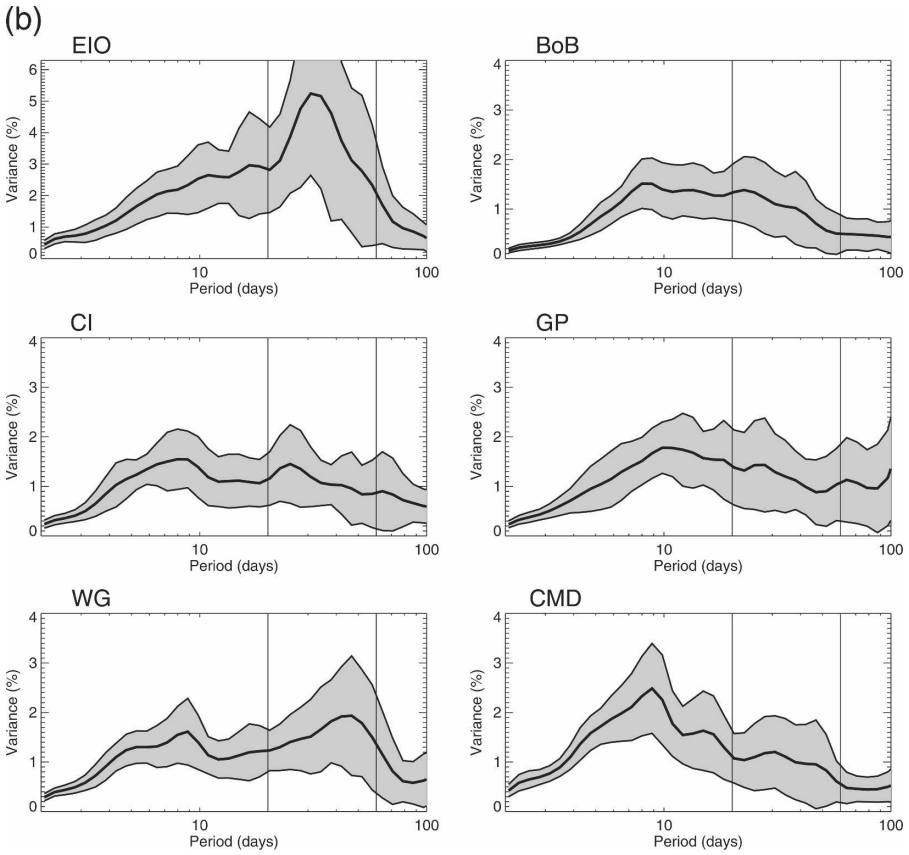

FIG. 3. (*Continued*)

and frequency localization of the distribution of the variance (power), it is possible to obtain a different average spectrum for every year (7 for GPCP rainfall, 26 for OLR). The mean average spectrum and the standard deviation of the spectrum are defined as the mean and the standard deviation of the power in all the yearly spectra for every period analyzed, respectively. The standard deviation is an indication of the variability of the periods in time as well as their change of amplitude. In general, rainfall in all regions shows high variability within a season on time scales ranging from about 7 to 60 days. Over EIO, the amplitude of the intraseasonal activity appears even stronger than the annual cycle, with a marked spectral peak at 30 days and a secondary peak around 15 days. This intraseasonal activity over the Indian Ocean is not an exclusive property of the summer season. In fact, variability in the intraseasonal band is usually stronger during winter (e.g., Salby and Hendon 1994). But, over most of the other regions considered, high intraseasonal activity is confined to the summer, with magnitude and periods that fluctuate notably from year to year as is evident in the average wavelet spectra and the magnitude of the deviation around the average. The intraseasonal activity during the wet phase of the Southeast Asian monsoon season is a well recognized feature since the work of Murakami (1976), Yasunari (1979), and Sikka and Gadgil (1980), who found intraseasonal variability associated with northward propagation of a zone of maximum cloudiness over the Indian Ocean. Since then, several studies (e.g., Cadet 1983; Krishnamurti and Subrahmanyam 1982; Knutson and Weickmann 1987; Hartmann and Michelsen 1989; Sengupta and Ravichandran 2001; Annamalai and Slingo 2001; Lawrence and Webster 2002) have reported the existence of intraseasonal spectral peaks in time series of precipitation, pressure, wind, OLR, and SST, as well as a tendency for northward propagation of the intraseasonal anomalies over the Indian Ocean.

From the summer average wavelet spectra, it is possible to identify some important aspects related to variability of rainfall within a wet summer season. For the BoB, in addition to the spectral peak corresponding to the annual cycle, there are two distinctive peaks at 10 and 30 days. A strong annual cycle peak is common to all regions except for the EIO. For CI, there are im-

portant spectral peaks at 6, 13, and 25 days, indicating significant variability differences with the BoB region.

While the wavelet spectrum of rainfall over the GP also shows intraseasonal 25–80-day variance during some years, it is not large enough to appear as a peak in the average spectrum. There is, however, a broad spectral peak between 4 and 9 days. The absence of a significant peak in the intraseasonal band poses a conundrum. Since the JJAS rainfall correlation is higher between the BoB and the GP than between the BoB and CI, why are the spectral characteristics of the variability closer between the BoB and CI?

For the WG, the average spectrum shows a broad peak between 5 and 50 days, indicating a more complicated temporal structure of the rainfall, perhaps due to the interaction between the combined effect of the large-scale monsoon intraseasonal variability and orography. Over CMD, the most distinctive peak after the annual cycle is located near 6 days (probably associated with propagating easterly waves from the Pacific Ocean) and a secondary peak around 45 days.

4. Intraseasonal variability during summer

The monsoon intraseasonal oscillation is the dominant large-scale feature of the monsoon (see review by Webster et al. 1998), which in general develops over the equatorial Indian Ocean and propagates eastward along the equator to the eastern reaches of the ocean (Yasunari 1979, 1981; Sikka and Gadgil 1980; Lawrence and Webster 2002; Webster and Hoyos 2004; Jiang et al. 2004). What local features modulate the intraseasonal monsoon rainfall signal so as to produce average spectra that are different in each region? Quite possibly the differences may depend on the specifics of the nature of the northward propagation, differences between individual oscillations, the different nature of the ocean–atmosphere in specific locations, and land–atmosphere feedbacks. In some manner, these processes aggregate to cause interannual variability of the intraseasonal mode.

Figure 4 shows the mean amplitude of the JJAS intraseasonal 25–80-day rainfall variance for each year from 1997 to 2004 as well as for all the years (multiannual). The mean amplitude in a spectral band is defined as the standard deviation of the filtered variable in the band, or alternatively, as the square root of the variance contained in the selected time span and spectral band. Areas of maximum intraseasonal activity vary strongly in magnitude and location from year to year, with the most recurrent feature being the high intraseasonal variability over the EIO and the BoB.

Figure 5 shows the cumulative intraseasonal rainfall for JJAS, obtained by simply adding the bandpassed rainfall time series for each day from 1 June to 30 September at every individual grid cell highlighting the locations where prolonged active and break phases of the monsoon occur. In essence, the distribution of positive and negative anomalies of rainfall associated with cumulative MISO activity can be regarded as the most important internal characteristic of interannual monsoon variability given its basinwide influence as well as the relative magnitude of the intraseasonal peak compared to variability at other time scales. Here we define internal variability as variability that does not arise through remote teleconnections with other phenomena, but rather from instabilities within the system. Among other sources of internal variability that could potentially introduce interannual monsoon anomalies are the variability at shorter time scales (e.g., 4–20-day variability) and the Indian Ocean Dipole (IOD; Saji et al. 1999; Webster et al. 1999). It is possible that the overall MISO activity during a season is partly modulated by long-term changes in the background state of the Indian Ocean induced by internal dynamics associated with the IOD, for example, or by external forcing such as ENSO. In the case that the former situation is true, the cumulative MISO would still be representing internally generated interannual variability. In the case of the latter, the cumulative MISO would be a mixture of internally and externally induced variability.

In the manner described above and similarly to Palmer (1994) and Webster et al. (1998), we hypothesize that summer intraseasonal activity, and especially its northward component, may be considered an instability of the monsoon system, which in general is not strongly affected by the changes in the long-term background state of the ocean–atmosphere system outside the Indian Ocean Basin and different teleconnections. The MISO occurs within the envelope of the summer monsoon, without preferred timing, and considerably altering the entire seasonal monsoon circulation. In addition, there exists outside the monsoon region no forcing of a time scale equal to that of the MISO. Little significant statistical relationship has been found between seasonal MJO activity and the ENSO cycle (Hendon et al. 2000; Slingo et al. 1999), except during extremely large warm events when MJO activity is suppressed. Hendon et al. (2000) suggested that most of the year-to-year variability of the MJO is internally generated independent of any slowly varying boundary forcing. In addition, Lawrence and Webster (2001) found that the summertime Intraseasonal Oscillation (ISO) is relatively uncorrelated with ENSO except for weakly positive correlation at the beginning of the

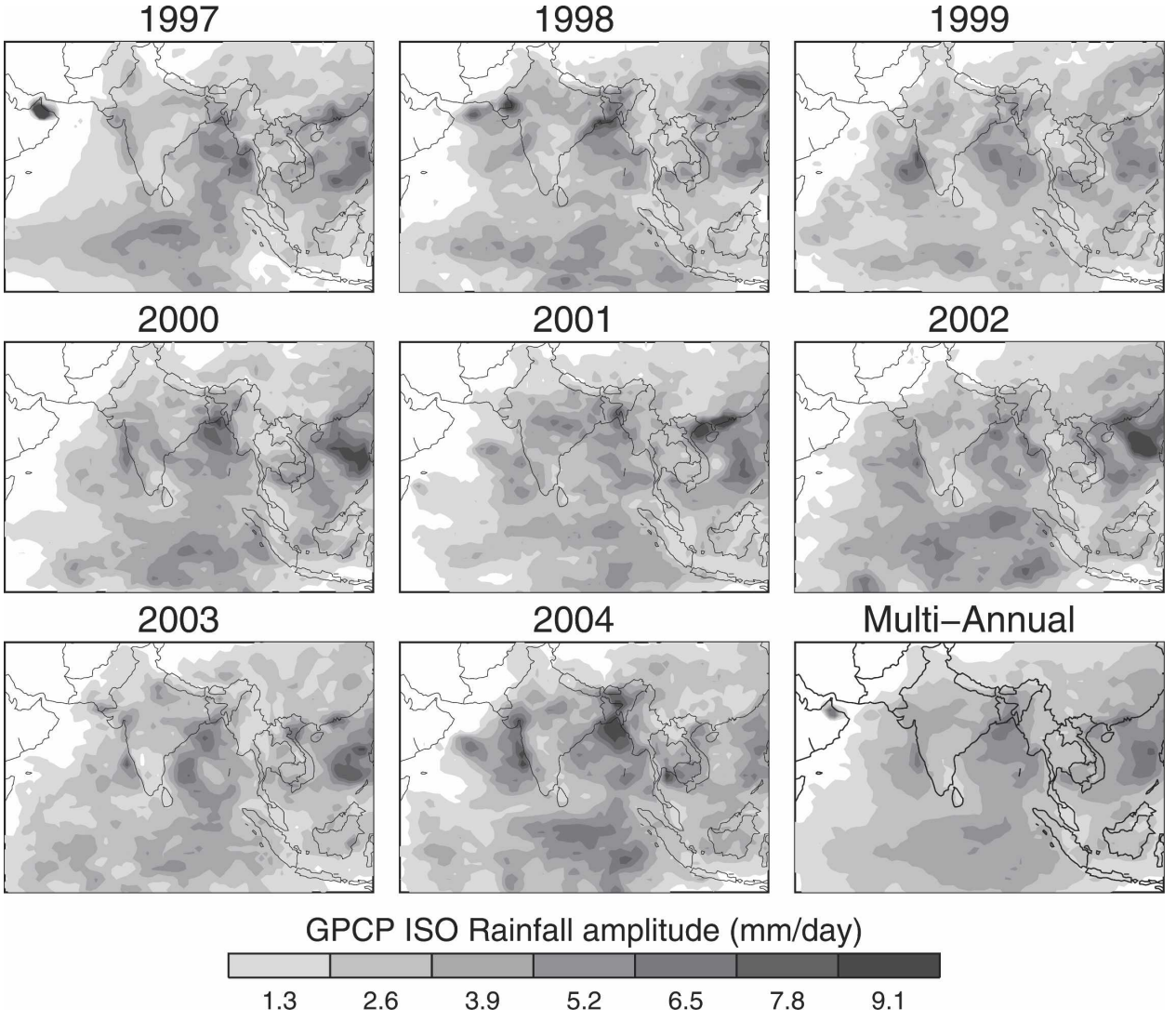

FIG. 4. Mean amplitude of the summer MISO (25–80 day) associated GPCP daily rainfall for each year from 1997 to 2004 as well as the multiannual average amplitude.

Southeast Asian monsoon season. As a consequence it appears that it is necessary to consider the distribution of the interannual internal variability in order to explain some of the spatial features of JJAS rainfall anomalies. Perhaps the most prominent variation from the average is the 2002 drought over India, which coincides with large amplitude negative anomalies of MISO rainfall over the Indian subcontinent, mainly occasioned by a very strong and prolonged midseason break. It is also important to note that Gadgil et al. (2004) show some evidence that in extreme cases, and in particular during 2002, a composite state of ENSO and the atmospheric component of the IOD suggest unfavorable conditions for the overall summer monsoon. From this point of view, 2002 is a good example of how external and internal forcing at different time scales played a role in determining the seasonal rainfall.

Figure 6 shows the variability of the 25–80-day bandpassed daily rainfall plotted against 4–20-day rainfall variance, for all maxima in a 4–20-day variance band and for all regions of the analysis (Fig. 1). Spectral analysis showed high variability in the 25–80- and 4–20-day bands in the regions of analysis. There are two major points that suggest that the variability in the 4–20-day band is mainly contained in the 25–80-day band, especially in the EIO, BoB, and CI. One is that the 4–20-day variance time series (not shown) presents intraseasonal variability, and the other is that, as observed in Fig. 6, most of the major peaks in the 4–20-day variance correspond to a maximum or a very high

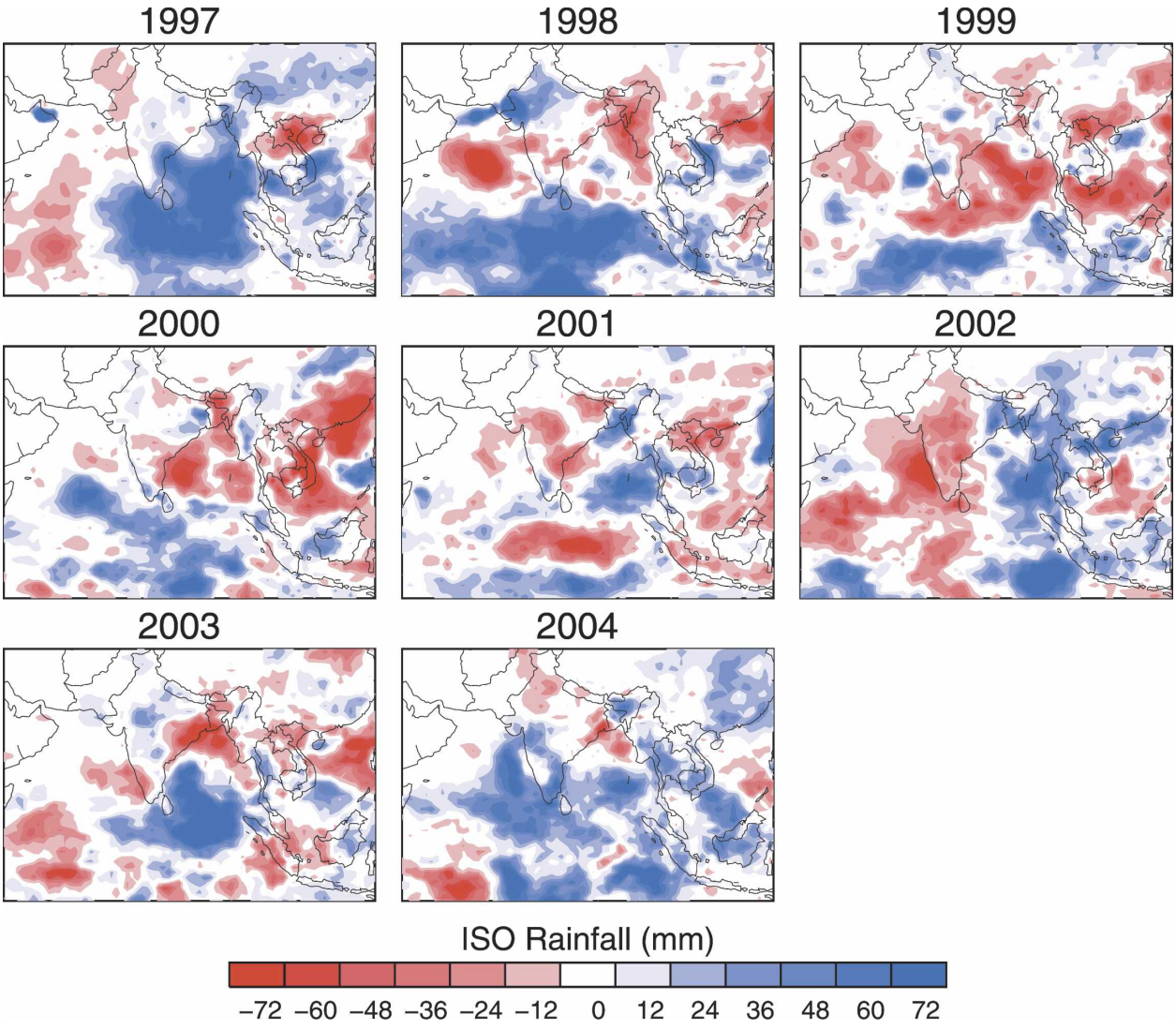

FIG. 5. Cumulative ISO (25–80 day) rainfall from the daily GPCP product during JJAS for each year from 1997 to 2004.

value (above 1 standard deviation) in the 25–80-day bandpassed rainfall. This indicates that rainfall variability in the 4–20-day band is preferentially present during active periods of the monsoon intraseasonal oscillation.

Similarly, most of the monsoon subsynoptic variability appears to be contained within the intraseasonal envelope of convection. Figure 7a shows the average wavelet spectrum of the 3-hourly TRMM rainfall over the BoB, illustrating in addition to the variability in the 4–20- and 25–80-day bands that there is a very strong diurnal cycle of precipitation. The amplitude of the diurnal cycle is modulated by the envelope of convection in the 4–20- and 25–80-day bands, with greater amplitude during the peak of the intraseasonal event (see Fig. 7b). Similarly, Goswami et al. (2003) showed that the genesis of the monsoon low pressure systems, with a typical time scale of 3–5 days, is strongly modulated by the MISO, being 3 times as likely in the active phase than during the suppressed phase.

5. Composite analysis of summer intraseasonal variability

The relatively regular behavior of the summer MISO (e.g., Webster et al. 1998; Lawrence and Webster 2002; Waliser et al. 2003a,b) has been used greatly in forecasting the discharge of the Ganges and Brahmaputra Rivers and regional rainfall over India (e.g., Goswami and Xavier 2003; Webster and Hoyos 2004). To study in detail the structure of the MISO over the Indian Ocean and Southeast Asia, the dates of maximum rainfall associated with intraseasonal activity (25–80-day bandpassed data) with magnitudes greater than 1 standard

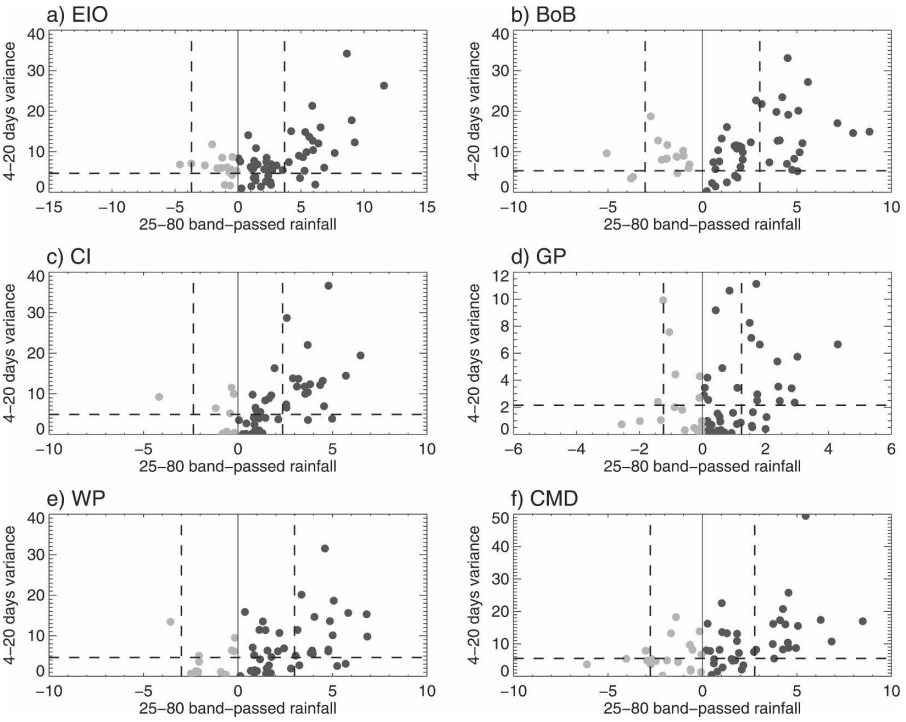

FIG. 6. The 25–80-day bandpassed daily GPCP rainfall (mm) plotted against 4–20-day rainfall variance (mm^2) for all maxima in 4–20-day variance for each region (Fig. 1). The horizontal dashed line represents 1 standard deviation of the 4–20-day rainfall variance and the vertical dashed lines represent ±1 standard deviation of 25–80-day rainfall. Dark (light) circles represent positive (negative) 25–80-day band rainfall anomalies.

deviation in the band were selected for the regions shown in Fig. 1. The composite evolution of several fields was studied. It was found that SST, surface pressure, lower-tropospheric winds, and rainfall itself (or OLR) emerge as the most coherent fields to explain the fundamental features of the intraseasonal activity.

For the BoB, a total of 24 cases were selected in the period 1997–2004. From those, 16 cases are classified as what may be referred to as the canonical MISO, 4 are classified as having developed in situ, and 4 as having developed through orographic interactions under break conditions over the Bay of Bengal.

a. BoB composites: Canonical MISO

Figures 8a–c show the composite behavior of 25–80-day bandpassed daily rainfall, 925-hPa winds and sea

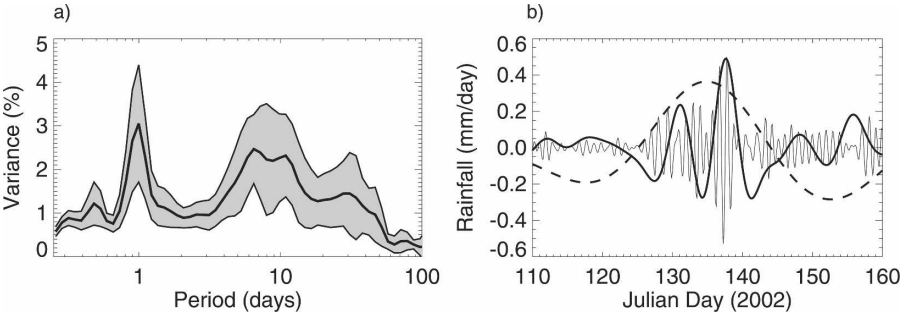

FIG. 7. (a) Average wavelet spectrum of the 3-hourly TRMM rainfall over the BoB from 1998 to 2004. The shaded region encloses the average spectrum ±1 standard deviation. (b) The 3-hourly TRMM rainfall variability in different time scales (bands) during one full intraseasonal event during summer 2002. The figure shows rainfall in the 25–80-day band (dashed line), 5–20-day band (thick solid line), and the diurnal cycle (thin solid line).

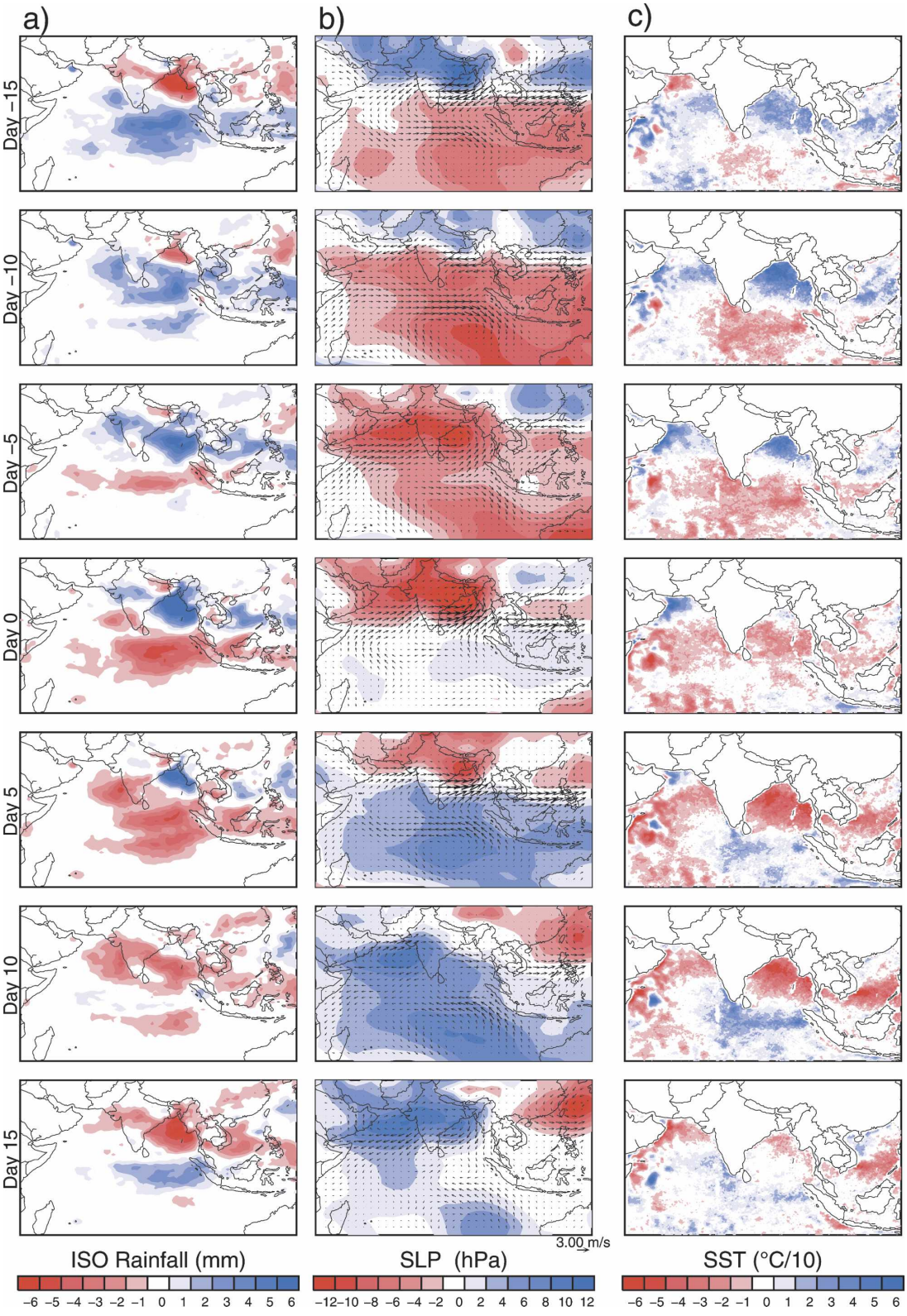

FIG. 8. Composites of 25–80-day bandpassed (a) GPCP daily rainfall, (b) 925-hPa winds and SLP from the NCEP–NCAR reanalysis, and (c) TMI SST for 16 canonical MISO events over BoB. Day −15 to +15; day 0 corresponds to the maximum MISO rainfall over the BoB.

level pressure (SLP), and SST, respectively, from suppressed to suppressed conditions over the BoB. The canonical structure corresponds to an intraseasonal event that starts as a convective anomaly in the equatorial Indian Ocean, followed by an eastward propagation that bifurcates with southward- and northward-propagating branches, usually off the west coast of Sumatra, introducing positive anomalies of precipitation over the BoB. The event develops (around day −20) over warm surface waters and low pressure at the equator. Around the same time, the BoB is under break (dry and suppressed) conditions associated with the previous MISO and high surface pressure with a corresponding anticyclonic circulation driving the air to the southwest over the bay away (perpendicularly) from the Burma mountains. The high pressure system is also seen in the Arabian Sea and India. These cloud-free conditions favor SST increases over the BoB and are integral parts of the MISO cycle (e.g., Stephens et al. 2004; Wang et al. 2005; Agudelo et al. 2006). The equatorial low-level surface pressure and associated convection propagates to the east, accompanied by surface cooling from freshening winds and increased surface evaporation. By the time the anomaly reaches the west coast of Sumatra (day −10), the waters at the north of the bay have warmed under the prior anticyclonic conditions, inducing the northward propagation of the surface low pressure from the equator, introducing positive anomalies of rainfall. The flow over the eastern side of the BoB is now parallel to the Burma mountains. As the MISO evolves, the surface low pressure center is located over India (day 0), driving moist air toward the eastern side of the bay and the Burma mountains (see Fig. 1) where orographic lifting enhances precipitation, resulting in the precipitation maximum aligned parallel to the mountain range (Fig. 2). By day +5, reductions in insolation and the freshening of winds cool the surface waters of the BoB, acting as a negative feedback on MISO convection. At about the same time, the following break phase starts to develop in the equatorial Indian Ocean induced largely by the subsidence of air and subsequent SST warming caused by convection farther north (Wang et al. 2005). The observed lags in convection in the composite pattern are corroborated by the estimation of wavelet coherency and phase lag between daily BoB and EIO rainfall (e.g., Torrence and Webster 1999). On average during the summers from 1997 to 2004, the mutual coherence in the intraseasonal 25–80-day band is 0.55 and their phase difference is about 120° (~15 days in this time scale), leading the rainfall over the EIO.

If we define an active phase as the time intervals where the rainfall anomalies in the 25–80-day band are positive on average in the period 1997–2004, 70% of the summer BoB precipitation falls during these active phases. In addition, if we consider the changes in the wind speed relative to the seasonal mean speed toward the Burma mountains (10 m s^{-1}), we find that on average MISO amplitude is about 6 m s^{-1}. That is, during an active period the wind speed is ~13 m s^{-1} and during a break the speed is ~7 m s^{-1}, corresponding to an increment of about 85% from break to active conditions. In addition, composites of unfiltered 925-mb winds relative to maximum MISO rainfall over the BoB (not shown) also reveal clearly the change of magnitude of the winds over the BoB. The combination of the northward propagation of the MISO with the considerable enhancement of the winds results in the observed maximum parallel to the mountains.

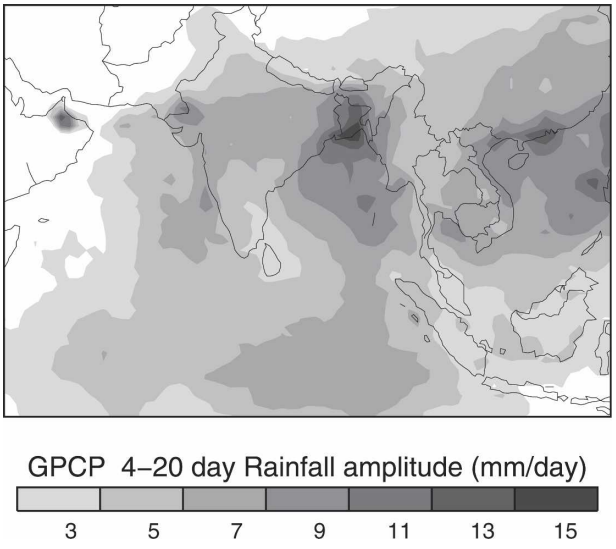

FIG. 9. Mean amplitude of the summer (JJAS) 4–20-day spectral band GPCP daily rainfall.

b. Variability within the BoB canonical MISO

Earlier, it was noted in Figs. 6 and 7 that the intraseasonal rainfall band contains higher frequency activity. We now consider this containment in greater detail.

Composite analysis of 64 intense precipitation events in the 4–20-day band (not shown) confirms that the higher-frequency events develop in situ mainly over the northern part of the BoB with no significant propagation and that about 75% of these events developed during MISO active conditions. Figure 9 displays the spatial distribution of the mean amplitude of the summer (JJAS) 4–20-day rainfall variability. The features are remarkably similar to the multiannual structure of intraseasonal variance shown in Fig. 4. This resemblance provides further evidence of the simultaneous coexistence of both modes of rainfall variability.

Figure 10 shows time–latitude sections of intraseasonal GPCP rainfall and 3-hourly TRMM rainfall for 2 strong MISO events occurring during May 1999 and May 2002. The features observed in these two examples are common for almost all events analyzed in the period 1998–2004. The diagram shows clearly the northward propagation of the envelope of convection from the equator enclosing individual southward-propagating storms possessing a marked diurnal cycle (as in Fig. 7). Webster et al. (2002) and Zuidema (2003) found similar propagating diurnal systems during the active phase by studying brightness temperature data during the Joint Air–Sea Monsoon Interaction Experiment (JASMINE) experiment (April–July 1999) and from Indian National Satellite (INSAT; summer 1998), as well as Meteosat-5 (summer 1999), respectively. The convection generally begins around midnight with decay around noon farther south (Zuidema 2003). According to Webster et al. (2002), these southward-propagating convective bands significantly perturb the surface fluxes and occasionally propagate into the Southern Hemisphere, redeveloping on the second night. The longer period of data considered in this work allow us to conclude that such southward-propagating storms are a robust feature of the active phases of the MISO over the BoB.

c. *In situ and orographically driven convection over the BoB*

In addition to the northward-propagating MISO, there is a class of disturbances that forms in situ in the BoB. These are very similar to the canonical type of intraseasonal variability but without the observed propagation either along the equator or poleward from the equator to the northern BoB, in contrast to the canonical form (Figs. 7–9). Rather, a dipolelike system is observed with positive anomalies of rainfall over the EIO and suppressed conditions over the BoB around day −20 and the reversed conditions at day 0. In this case, warm surface waters in the BoB induce convection, eroding the high sea level pressure established during the suppressed phase and allowing the formation of the low pressure system.

In the intraseasonal band, there is a sequence of low and high pressure systems associated with active and break phases, respectively. Under special conditions of stability and atmospheric moisture over the BoB, and a correct location of the high pressure system, orographically uplift-producing rainfall is possible. Specifically, a high pressure system situated to the south of the BoB generates an anticyclonic circulation that drives the air toward the Burma mountain range, where the air is mechanically lifted, setting up the conditions for rainfall over the bay. Figure 11 shows the evolution of the 25–80-day bandpassed rainfall, SLP, and 925-hPa winds for a case where rainfall was orographically induced. Day 0 corresponds to 17 June 2003. Given the fact that only four of these cases were identified in the period 1997–2004, it is better to show a particular case than the composite structure based on a few cases. The figure clearly shows break conditions over the BoB around day −20, with negative anomalies of rainfall and positive anomalies of SLP. At day −15, the high pressure center is located in the southern part of the BoB around 8°–10°N, establishing that an anticyclonic circulation produces flow toward the mountains near the border of Burma and Bangladesh, forcing ascent resulting in rainfall. After day 0 (not shown), the rainfall system propagates northwestward, generating positive rainfall anomalies over GP. Figure 11c shows the horizontal cross section of the raw near-surface rainfall rate (TRMM 2A25–V6 product) and QuikSCAT winds over the BoB during day −7 (10 June 2003), as well as the vertical distribution of rainfall along the central line of the retrieval. These figures illustrate the direct influence of the topography in the generation of rainfall over the eastern margin of the BoB during large-scale suppressed conditions. While this type of rainfall over the BoB in the intraseasonal band is not as common as the canonical type, it still contributes to the seasonal maximum over the bay.

d. *Regional impacts of the canonical MISO*

The canonical monsoon intraseasonal oscillation not only affects the rainfall over the BoB, but also over CI, GP, WG, and even CMD. Figure 12 shows composite time–latitude diagrams of 25–80-day bandpassed rainfall, SLP and zonal winds, and SST from day −25 to day 15 for the selected active MISO events over BoB (16 events), CI (15), GP (10), WG (18), and CMD (12). To study the main differences in the intraseasonal oscillation propagation that affect different regions, the time–latitude diagrams are constructed for different longitude spans, 65°–75°E, 75°–85°E, and 85°–95°E. While the canonical monsoon intraseasonal oscillation is a relatively repeatable large-scale phenomenon, the MISO evolution occurs in such a way that in some cases the maximum convective activity is located over the BoB, while in other cases over CI or other regions. Possibly, small differences in the background state are responsible for these differences in the MISO propagation. The general feature observed in the figures is the northward propagation of the convective envelope, including signals in the precipitation, sea level pressure, zonal winds, and SST fields.

The composite structure based on the activity over

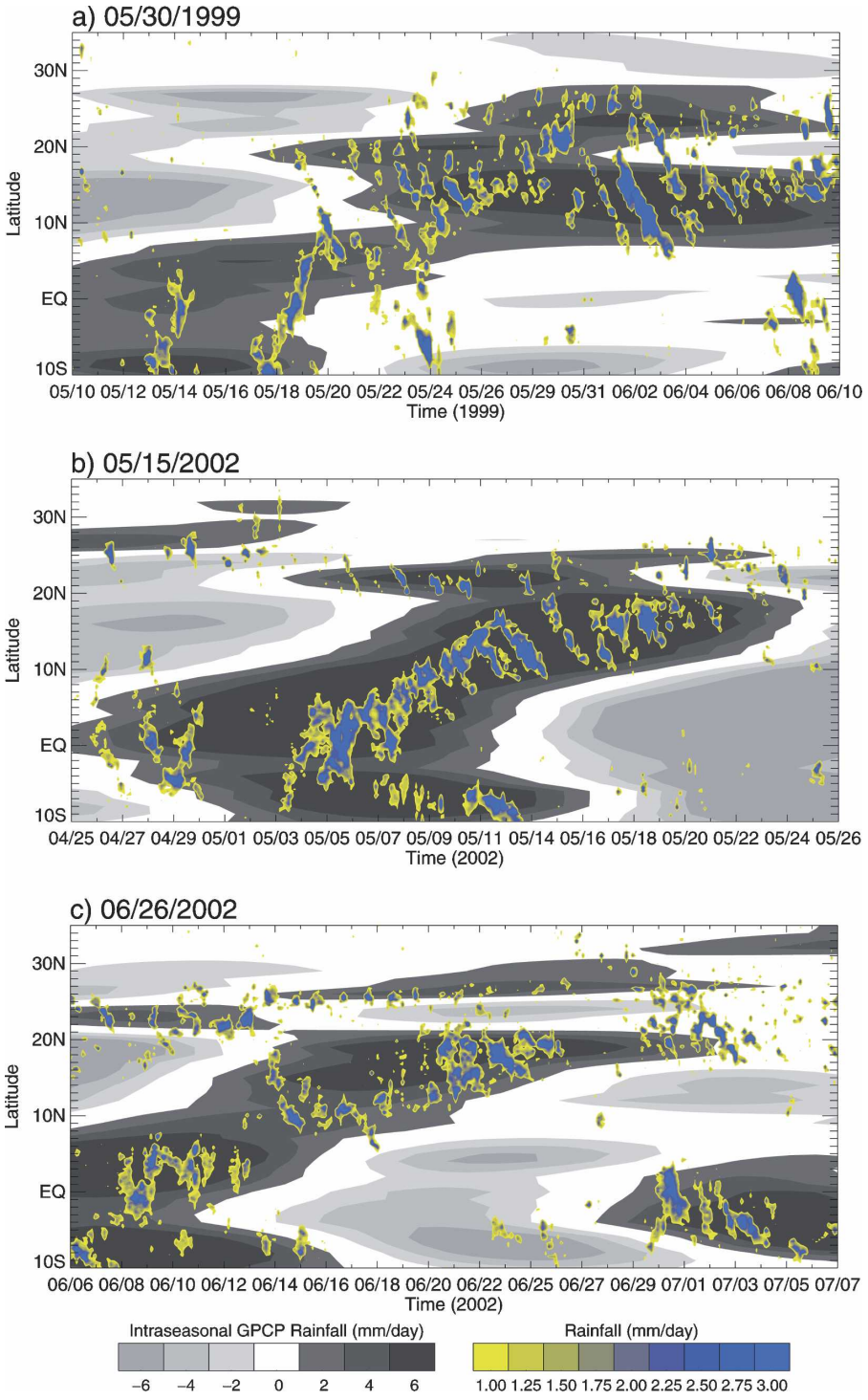

FIG. 10. Time–latitude diagram of intraseasonal (25–80 day) GPCP rainfall shown in grayscale and 3-hourly TRMM rainfall in yellow/blue color for three maximum events over the BoB: (a) 30 May 1999, (b) 15 May 2002, and (c) 26 Jun 2002.

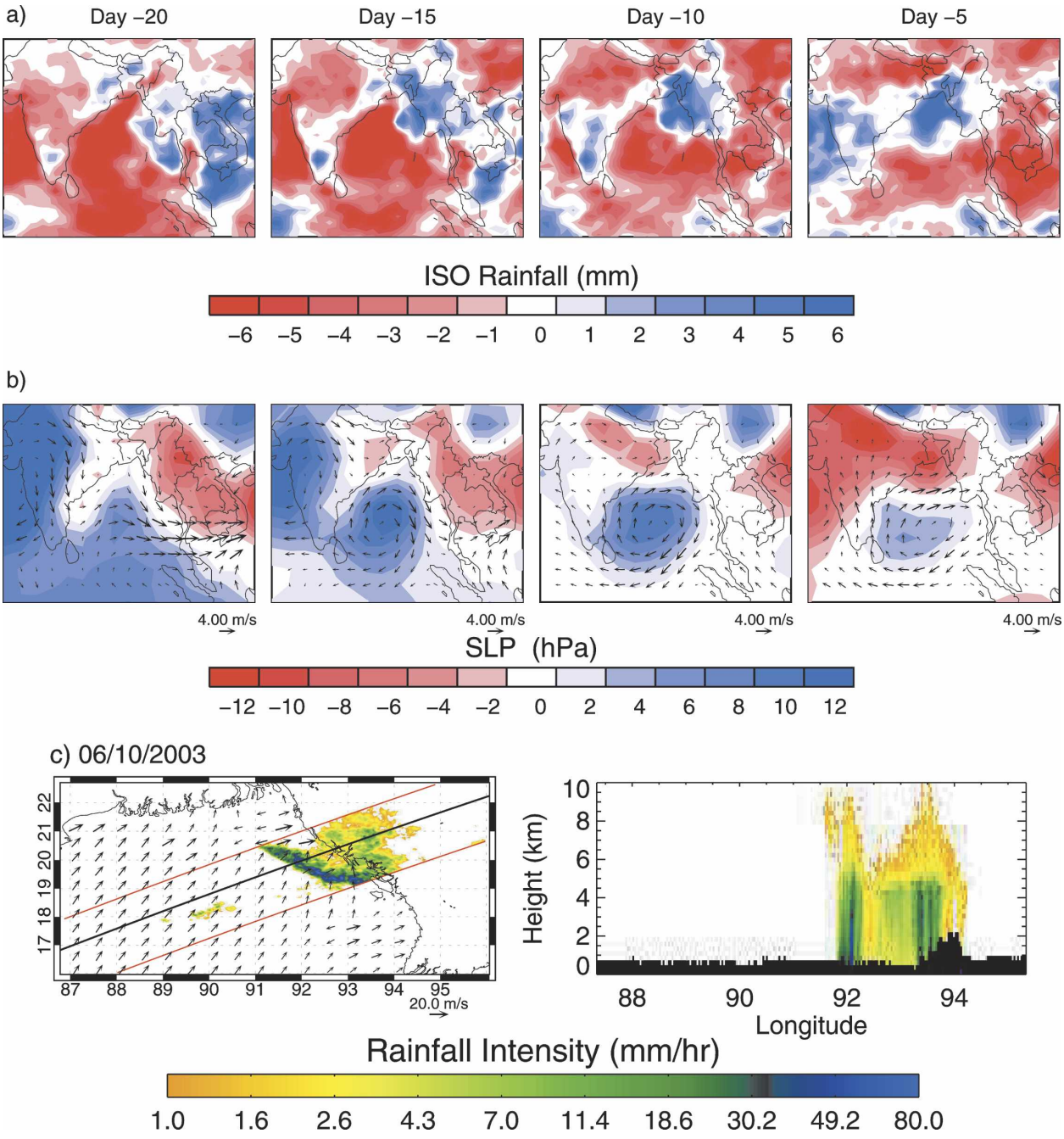

FIG. 11. Evolution of 25–80-day (ISO) bandpassed (a) GPCP rainfall and (b) NCEP–NCAR SLP and 925-hPa winds showing orographically driven precipitation. Day 0 corresponds to 17 Jun 2003. (c) (left) Horizontal (lat–lon) cross section of near-surface rainfall rate (TRMM 2A25–V6 product) over the BoB and QuikSCAT winds on 10 Jun 2003, and (right) vertical distribution of rainfall along the black diagonal line shown in left panel (measurements are only available inside the red lines). The black shading at the bottom of (c) (right) indicates no retrieval.

the BoB shows positive intraseasonal variability anomalies of SST leading the equatorial development and northward propagation of the enhanced convection. The low pressure anomaly propagates simultaneously with and at approximately the same speed as the rainfall anomalies, while the lower-tropospheric zonal wind anomalies appear to propagate at a slower pace. This is an important observation for the potential prediction of active and break phases of the Southeast Asian monsoon since slower propagation directly implies more

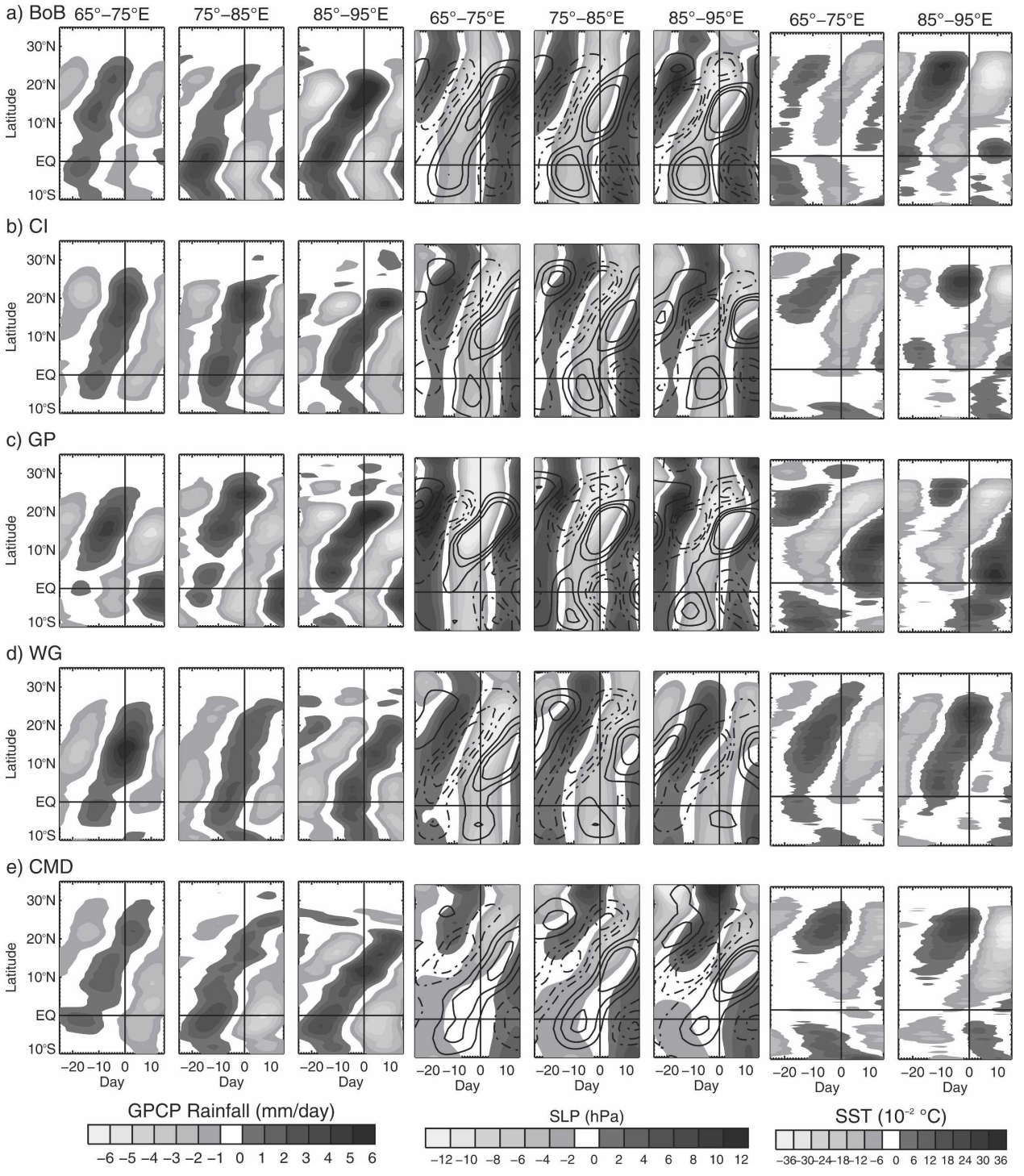

FIG. 12. Composite time–latitude diagrams for longitudes 65°–75°E, 75°–85°E, and 85°–95°E of 25–80-day bandpassed (left three columns) GPCP rainfall, (middle three columns) SLP and zonal winds, and (right two columns, longitudes 75°–85°E not shown) SST from day −25 to day 15 for (a) BoB (16 events), (b) CI (15), (c) GP (10), (d) WG (18), and (e) CMD (12). In middle three columns, solid (dashed) contours represent westerly (easterly) winds, and the magnitudes are 0.5, 1.0, and 1.5 m s^{-1}.

memory in the dynamical system and hence higher predictability. For the BoB composites, the propagation of sea level pressure and wind anomalies is strong in all longitude bands in the Indian Ocean (65°–75°E, 75°–85°E, and 85°–95°E) and is representative of the large-scale dynamical features of the MISO. However, these anomalies are weak over Sumatra (95°–105°E; not shown), where the convective signal fades. On the other hand, the strongest convective signal is largely confined to the 85°–95°E longitudinal band. Northward propagation of convection is also observed in the other longitudinal bands but with much weaker amplitude. A similar structure is observed in the SST fields, where the signal over 85°–95°E is much stronger than over 65°–75°E. The composites for CI show a very similar structure of SLP and lower-troposphere zonal winds to the BoB and more homogeneous convective activity and SST signals over the Indian Ocean. For the GP, the 75°–85°E time–latitude diagram shows that the convective anomaly penetrates farther north than the average canonical MISO events. In this case, the SST diagrams show a much slower propagation of the MISO-related anomalies.

For the WG composites, the sea level pressure, zonal wind, and precipitation anomalies are strong on the west side of the Indian Ocean, suggesting an earlier northward propagation and precipitation compared to the canonical MISO over the BoB. The SST diagrams in this case show similar features in the west and east sides of the Indian Ocean. The composites for Cambodia show, in general, a much weaker propagating signal in all variables, in part because the convective signal tends to bifurcate before reaching Sumatra and to weaken farther east.

Interregional correlations in the intraseasonal band also confirm some of the propagation features observed in the composites. The correlation between EIO and BoB summer filtered rainfall (0.6) confirms that rainfall over the EIO leads rainfall over the BoB by approximately 16 days (lag of maximum correlation). In a similar manner, the correlation (0.32 and 0.43) indicates that rainfall over the EIO leads CMD and CI by about 17 and 8 days, respectively. The correlation suggests that most of the convective events that bifurcate in the EIO reach the BoB but not CMD. In addition, in occasions when the bifurcation takes place in EIO, convective anomalies have already started their northward propagation over the central Indian Ocean, explaining the lower lead time between EIO and CI than between EIO and BoB. BoB and WG are poorly correlated (0.23) with a lead time of 3 days for WG, suggesting that they are rarely affected by the same event. Rainfall over CI leads for about 7 days the anomalies at BoB (0.46) and the GP for about 2 days with a very high correlation (0.72), and BoB rainfall leads GP for about 4 days (0.51). The high correlation between CI and GP indicates that most of the intraseasonal events that reach CI also reach GP but generate considerably less anomalies. Events that reach the BoB on occasion reach the GP or establish the intraseasonal envelope for the westward propagation of anomalies in the 4–20-day band.

e. Other noncanonical MISOs

In addition to the positive anomalies of rainfall introduced by the canonical MISO, localized anomalies also need to be considered in the GP, CI, and over the BoB. In general, when positive rainfall anomalies grow over these regions, suppressed conditions are established over the equatorial Indian Ocean in a dipolelike structure.

Over CMD, besides the canonical MISO, 25–80-day activity also grows to the northeast of Indonesia and propagates westward, modulating rainfall over CMD and surrounding countries. The westward-propagating high pressure system generates an anticyclonic circulation to the east of Vietnam. In the longitude–time diagrams, this circulation appears as an easterly anomaly since the zonal winds are averaged over the southern half of the high. The inverse situation is observed with the propagation of the surface low. In this case, positive, nonpropagating anomalies of SST lead the development of the instability and the subsequent propagation.

f. The 4–20-day variability

On the 4–20-day time scale, the variability over the northeast BoB and WG develops predominantly in an in situ fashion. Figure 13 shows a composite structure from 51 events over CI. The figure displays a coherent westward propagation of positive convective anomalies and corresponding low pressure systems toward CI from the Gulf of Thailand and the South China Sea, affecting rainfall in the south and central BoB. These results are in agreement with the findings of Annamalai and Slingo (2001) and Krishnamurti and Ardanuy (1980). In some of the strongest cases in the composite set, the anomalies reach the Arabian Sea. The SST composite evolution suggests relatively small positive SST anomalies over the BoB leading the propagation of the convective system. The magnitude of the SST variability in this band is smaller than the amplitude in the 25–80-day band, suggesting a weaker ocean–atmosphere coupling/interaction in the 4–20-day band. The 51 CI events were reclassified as occurring during active or break MISO periods to evaluate possible differ-

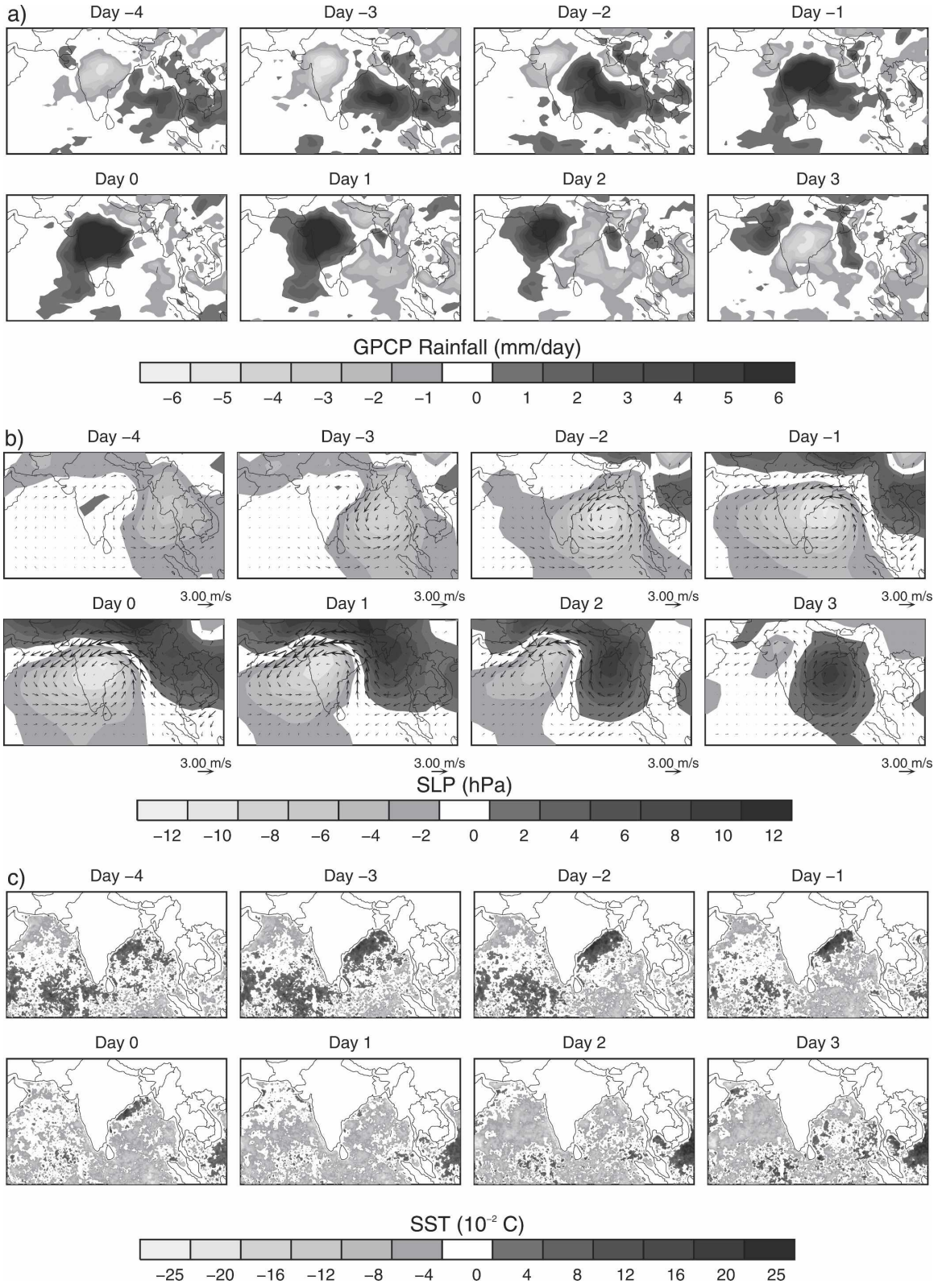

FIG. 13. Composites of the 5–25-day bandpassed (a) GPCP daily rainfall, (b) SLP and zonal winds, and (c) SST for 51 westward-propagating events over CI: Day −4 to +3; day 0 corresponds to the maximum rainfall in the band.

ences. In total, 31 events coincide with an active phase and 19 with a suppressed phase, confirming the fact that higher-frequency variability occurs within the MISO envelope. The reclassified composite structure does not show any significant differences in the westward propagation.

Figure 14 shows the composite structure for the 55 CMD cases, with a developing instability to the east of the Philippines that subsequently propagates to the west, generating copious rainfall over CMD and surrounding countries. These events also tend to reach the south of the BoB and, in some cases, the Indian subcontinent. When the instability is in its initial stages, the South China Sea possesses positive anomalies of SST that lead the westward propagation. In a similar manner to the CI case, the magnitude of the anomalies is relatively small. Overall, variability in the 4–20-day band over CMD shows a similar structure to that previously explained for the 25–80-day time scale.

6. Conclusions

A variety of data sources were used to study the contribution of rainfall variability over a range of time scales to the long-term mean seasonal summer (JJAS) monsoon rainfall (Fig. 2a). The role of the MISO in generating internal interannual variability of the monsoon system was also studied.

It was shown that both the amplitude and the distribution of the cumulative MISO-related rainfall strongly vary from year to year, constituting one of the most important sources of internal monsoon interannual variability. To a large degree, this internal variability is required to explain many important features of the seasonal rainfall distribution. In addition, the low values of the interregional correlation of rainfall within the monsoon system (Table 1) suggest large internal monsoon variability. Collectively, these factors introduce a scientific challenge for all teleconnection studies. To evaluate the effect and/or mutual influence among the monsoon and different external forcing phenomena (e.g., ENSO), it is necessary to design and evaluate tools that separate internal from external interannual variability. Statistically, it is difficult to separate internal and external sources of interannual variability from datasets because of the relatively short high-resolution and spatially distributed data available; however, ensemble model experiments could be used for that purpose (e.g., Quan et al. 2004).

To obtain a better understanding of the nature of the intraseasonal activity over the Southeast Asian monsoon region and its effect on the distribution of rainfall, a detailed composite analysis was undertaken based on strong MISO events over six key regions for the monsoon. Emerging from the composite analysis is the most coherent temporal and spatial structure of the MISO instability. The structure was referred to as the canonical MISO and is shown schematically in Figs. 15a,b. This mode starts in the equatorial Indian Ocean following warmer than average surface waters. Anomalies then generally propagate eastward to the EIO where they bifurcate, generating sequential active and break periods over all the regions considered, even as far east as CMD. The northward propagation of the convective anomalies, accompanied by a low pressure system, lags the propagation of the SST anomalies. The variability within the convective MISO envelope, especially over the BoB, shows individual southward-propagating storms with life spans less than a day (Fig. 10).

It was noted that large-scale ocean–land temperature gradients cannot explain the mean seasonal precipitation patterns and are especially unrelated to the BoB precipitation maximum. However, the strongest canonical MISO signal occurs over the BoB, following the bifurcation of the near-equatorial convective anomalies to the west of Sumatra. After the northward propagation of the low pressure system, the center of the latter is positioned over India, generating cyclonic circulation that tends to drive moist air toward the Burma mountain range, which possesses an average elevation of about 1800 m. Upstream effects of mountain ranges considerably enhance rainfall over the ocean in the northeast corner of the Bay of Bengal, explaining much of the observed seasonal maximum parallel to the mountains. The mountains of Burma do not seem to play a defining role in the MISO evolution itself, nor in the northward propagations, but it would seem that they directly influence the cumulative MISO-associated rainfall and, hence, the magnitude of the observed seasonal rainfall.

Other studies (Grossman and Durran 1984; Grossman and Garcia 1990; Xie et al. 2006) have noted the importance of orographic features in the spatial organization of the monsoon rainfall. However, where this study differs in particular is that it considers the interaction of orography with a variety of circulation patterns of different time scales. Xie et al. (2006), for example, used monthly precipitation and excluded by this choice important intraseasonal time scales. In this work, we specifically identified the interaction of the MISO during both active and suppressed conditions with orography in order to recognize the specific cause of precipitation over the Bay of Bengal.

The determination of the important role of the interaction between the MISO and orography is an important result since it suggests that in order for the climate

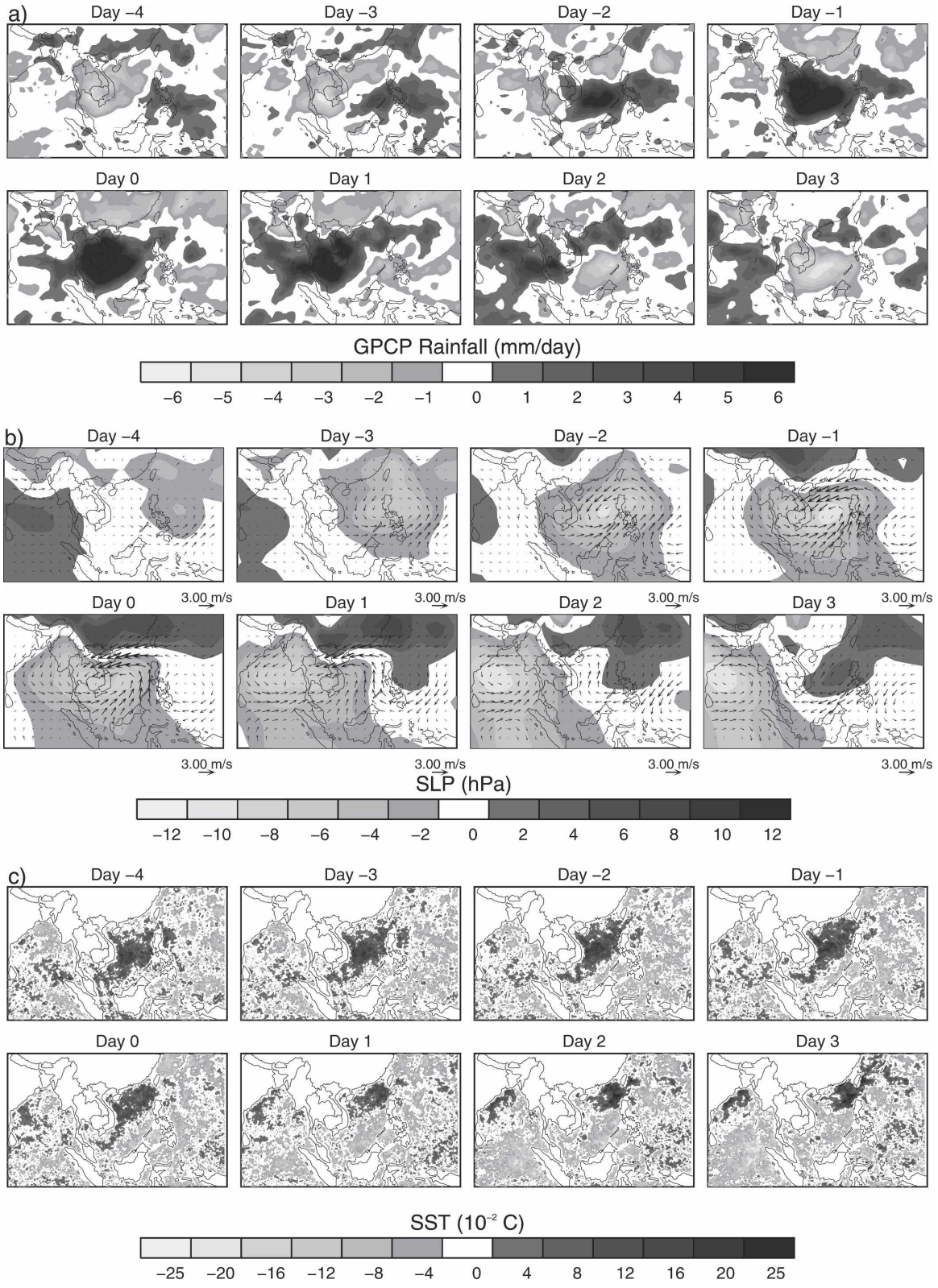

FIG. 14. Same as in Fig. 13 but for 55 events in the CMD region.

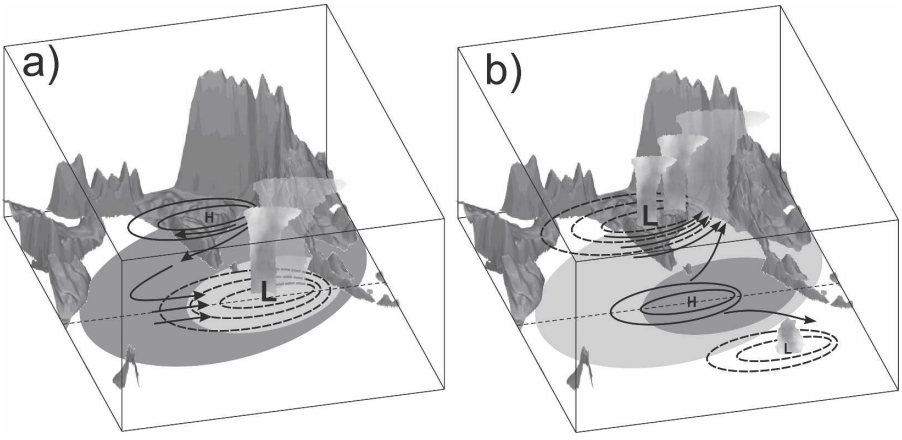

FIG. 15. Schematic diagram of the development of rainfall over the BoB associated with the ISO. The canonical monsoon ISO is shown: (a) start of mode and (b) bifurcation and northward propagation. Shaded areas over the ocean indicate the relative magnitude of the SST with the darker (clearer) shading showing warmer (colder) than usual SST. The H (L) and the solid (dashed) contours indicate a surface high (low). The arrows indicate the direction of the surface winds.

models to reproduce the observed seasonal monsoon rainfall structure, they need to simulate better the intraseasonal activity observed and also be able to include the important effects of tall narrow mountains.

The study identified why there is regional precipitation occurring from time to time over the bay during break conditions over northern India. This occurs when a high pressure system is located in the south of the bay, inducing an anticyclonic circulation that drives moist air toward the mountains near the Bangladesh–Burma border. This sequence is described schematically in Figs. 16a,b. Under the proper conditions of atmospheric stability and moisture, orographically induced rainfall develops, augmenting the seasonal rainfall parallel to the mountains.

In addition to the canonical MISO, in situ activity can develop over CI, the GP, and the BoB. Over CMD, westward-propagating disturbances developing to the east of the Philippines also generate rainfall both in the 25–80- and 4–20-day bands. The main difference in these 2 cases is that in the 25–80-day band, the SST variability is higher, suggesting stronger ocean–atmosphere coupling in this band compared to the 4–20-day band. Over CI, activity on the 4–20-day time scale also comes from the east with propagating disturbances generated over the Gulf of Thailand and South China Sea.

It is quite possible that due to the sensitivity of models to initial conditions and the nonlinear nature of a MISO event, models will not be able to forecast more than one MISO event ahead of time. As a consequence,

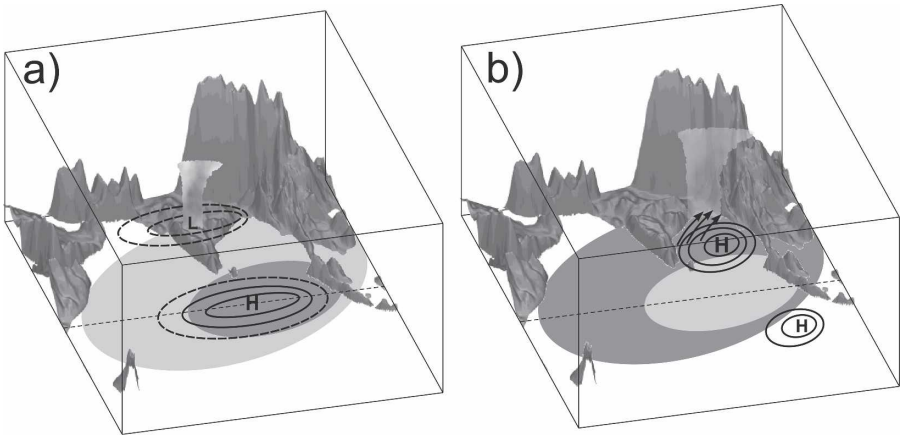

FIG. 16. Same as in Fig. 15 but for the orographic development of rainfall during break conditions. The figure describes the (a) origin and (b) propagation of the suppressed phase.

the full MISO activity during the summer season cannot be completely anticipated. However, because of the regular and coherent nature of the MISO, in order to estimate better the spatial structure of the seasonal rainfall, a summary of the statistical nature of intraseasonal activity prior to the summer season may help. Such a statistical quantification of the MISO would have to come from a model that is able to sustain intraseasonal variance with a magnitude similar to that observed. Wang and LinHo (2002) reached a similar conclusion when studying the features of the rainy season of the entire Asian–Pacific domain, noting that "an adequate description of the spatial–temporal structure of the mean Asian–Pacific monsoon rainy season should take the intrinsic subseasonal components into account."

This study of the subseasonal rainfall variability has provided some key aspects that help in understanding the processes that determine the seasonal distribution of summer monsoon rainfall. Much work is still required to understand the role of the background state on individual intraseasonal event propagation. While the large-scale dynamical features of a MISO appear to be very robust, the background state may affect rainfall in one region and not the others. Collectively, a deeper understanding is needed for both empirical forecasting of monsoon rainfall and for determining model standards for numerical prediction.

Acknowledgments. This research has been supported by the Climate Dynamics Division of the National Science Foundation under Award NSF-ATM 0531771.

REFERENCES

Adler, R. F., G. J. Huffman, D. T. Bolvin, S. Curtis, and E. J. Nelkin, 2000: Tropical rainfall distributions determined using TRMM combined with other satellite and rain gauge information. *J. Appl. Meteor.,* **39,** 2007–2023.

——, and Coauthors, 2003: The Version-2 Global Precipitation Climatology Project (GPCP) monthly precipitation analysis (1979–present). *J. Hydrometeor.,* **4,** 1147–1167.

Agudelo, P. A., J. A. Curry, C. D. Hoyos, and P. J. Webster, 2006: Transition between suppressed and active phases of intraseasonal oscillations in the Indo-Pacific warm pool. *J. Climate,* **19,** 5519–5530.

Annamalai, H., and J. M. Slingo, 2001: Active/break cycles: Diagnosis of the intraseasonal variability of the Asian summer monsoon. *Climate Dyn.,* **18,** 85–102.

Cadet, D., 1983: The monsoon over the Indian Ocean during summer 1975. Part II: Break and active monsoons. *Mon. Wea. Rev.,* **111,** 95–108.

Gadgil, S., and S. Sanjani, 1998: Monsoon precipitation in the AMIP runs. *Climate Dyn.,* **14,** 659–689.

——, Y. P. Abrol, and P. R. Seshagiri Rao, 1999: On growth and fluctuation of Indian foodgrain production. *Curr. Sci.,* **76,** 548–556.

——, P. R. Seshagiri Rao, and K. Narahari Rao, 2002: Use of climate information for farm-level decision making. *Agric. Syst.,* **74,** 431–457.

——, P. N. Vinayachandran, P. A. Francis, and S. Gadgil, 2004: Extremes of the Indian summer monsoon rainfall, ENSO and equatorial Indian Ocean oscillation. *Geophys. Res. Lett.,* **31,** L12213, doi:10.1029/2004GL019733.

Goswami, B. N., and P. K. Xavier, 2003: Potential predictability and extended range prediction of Indian summer monsoon breaks. *Geophys. Res. Lett.,* **30,** 1966, doi:10.1029/2003GL017810.

——, R. S. Ajayamohan, P. K. Xavier, and D. Sengupta, 2003: Clustering of synoptic activity by Indian summer monsoon intraseasonal oscillations. *Geophys. Res. Lett.,* **30,** 1431, doi:10.1029/2002GL016734.

Grossman, R. L., and D. R. Durran, 1984: Interaction of low-level flow with the Western Ghat Mountains and offshore convection in the summer monsoon. *Mon. Wea. Rev.,* **112,** 652–672.

——, and O. Garcia, 1990: The distribution of deep convection over ocean and land during the Asian summer monsoon. *J. Climate,* **3,** 1032–1044.

Hartmann, D. L., and M. L. Michelsen, 1989: Intraseasonal periodicities in Indian rainfall. *J. Atmos. Sci.,* **46,** 2838–2862.

Hendon, H. H., B. Liebmann, M. Newman, J. D. Glick, and J. E. Schemm, 2000: Medium-range forecast errors associated with active episodes of the Madden–Julian oscillation. *Mon. Wea. Rev.,* **128,** 69–86.

Huffman, G. J., and Coauthors, 1997: The Global Precipitation Climatology Project (GPCP) combined precipitation dataset. *Bull. Amer. Meteor. Soc.,* **78,** 5–20.

——, R. F. Adler, M. M. Morrissey, D. T. Bolvin, S. Curtis, R. Joyce, B. McGavock, and J. Susskind, 2001: Global precipitation at one-degree daily resolution from multisatellite observations. *J. Hydrometeor.,* **2,** 36–50.

Jiang, X., T. Li, and B. Wang, 2004: Structures and mechanisms of the northward propagating boreal summer intraseasonal oscillation. *J. Climate,* **17,** 1022–1039.

Kalnay, E., and Coauthors, 1996: The NCEP/NCAR 40-Year Reanalysis Project. *Bull. Amer. Meteor. Soc.,* **77,** 437–471.

Kirtman, B. P., and J. Shukla, 2000: On the influence of the Indian summer monsoon on ENSO. *Quart. J. Roy. Meteor. Soc.,* **126,** 213–239.

Knutson, T. R., and K. M. Weickmann, 1987: 30–60 day atmospheric oscillations: Composite life cycles of convection and circulation anomalies. *Mon. Wea. Rev.,* **115,** 1407–1436.

Krishnamurti, T. N., and P. Ardanuy, 1980: The 10 to 20 day westward propagating mode and "breaks in the monsoon." *Tellus,* **32,** 15–26.

——, and D. Subrahmanyam, 1982: The 30–50 day mode at 850 mb during MONEX. *J. Atmos. Sci.,* **39,** 2088–2095.

Kumar, K. K., B. Rajagopalan, and M. A. Cane, 1999: On the weakening relationship between the Indian monsoon and ENSO. *Science,* **284,** 2156–2159.

Lal, M., K. K. Singh, G. Srinivasan, L. S. Rathore, D. Naidu, and C. N. Tripathi, 1999: Growth and yield responses of soybean in Madhya Pradesh, India to climate variability and change. *Agric. For. Meteor.,* **93,** 53–70.

Lawrence, D. M., and P. J. Webster, 2001: Interannual variations of the intraseasonal oscillation in the South Asian summer monsoon region. *J. Climate,* **14,** 2910–2922.

——, and ——, 2002: The boreal summer intraseasonal oscilla-

tion: Relationship between northward and eastward movement of convection. *J. Atmos. Sci.,* **59,** 1593–1606.

Liebmann, B., and C. A. Smith, 1996: Description of a complete (interpolated) outgoing longwave radiation dataset. *Bull. Amer. Meteor. Soc.,* **77,** 1275–1277.

Murakami, T., 1976: Cloudiness fluctuations during the summer monsoon. *J. Meteor. Soc. Japan,* **54,** 175–181.

Palmer, T. N., 1994: Chaos and predictability in forecasting the monsoons. *Proc. Indian Natl. Sci. Acad.,* **60A,** 57–66.

Parthasarathy, B., N. A. Sontakke, A. A. Munot, and D. R. Kothawale, 1987: Droughts/floods in the summer monsoon rainfall season over different meteorological subdivisions of India for the period 1871–1984. *J. Climatol.,* **7,** 57–70.

——, A. A. Munot, and D. R. Kothawale, 1988: Regression model for estimation of Indian food grain production from Indian summer rainfall. *Agric. For. Meteor.,* **42,** 167–182.

Quan, X. W., P. J. Webster, A. M. Moore, and H. R. Chang, 2004: Seasonality in SST-forced atmospheric short-term climate predictability. *J. Climate,* **17,** 3090–3108.

Saji, N. H., B. N. Goswami, P. N. Vinayachandran, and T. Yamagata, 1999: A dipole mode in the tropical Indian Ocean. *Nature,* **401,** 360–363.

Salby, M. L., and H. H. Hendon, 1994: Intraseasonal behavior of clouds, temperature, and motion in the Tropics. *J. Atmos. Sci.,* **51,** 2207–2224.

Sengupta, D., and M. Ravichandran, 2001: Oscillations of Bay of Bengal sea surface temperature during the 1998 summer monsoon. *Geophys. Res. Lett.,* **28,** 2033–2036.

Sikka, D. R., and S. Gadgil, 1980: On the maximum cloud zone and the ITCZ over Indian longitudes during the southwest monsoon. *Mon. Wea. Rev.,* **108,** 1840–1853.

Slingo, D., P. Rowell, K. R. Sperber, and F. Nortley, 1999: On the predictability of the interannual behavior of the Madden–Julian oscillation and its relationship with El Niño. *Quart. J. Roy. Meteor. Soc.,* **125,** 583–609.

Sperber, K. R., and T. N. Palmer, 1996: Interannual tropical rainfall variability in general circulation model simulations associated with the Atmospheric Model Intercomparison Project. *J. Climate,* **9,** 2727–2750.

Stephens, G. L., P. J. Webster, R. H. Johnson, R. Engelen, and T. L'Ecuyer, 2004: Observational evidence for the mutual regulation of the tropical hydrological cycle and tropical sea surface temperatures. *J. Climate,* **17,** 2213–2224.

Torrence, C., and G. P. Compo, 1998: A practical guide to wavelet analysis. *Bull. Amer. Meteor. Soc.,* **79,** 61–78.

——, and P. J. Webster, 1999: Interdecadal changes in the ENSO–monsoon system. *J. Climate,* **12,** 2679–2690.

Waliser, D. E., W. Stern, S. Schubert, and K. M. Lau, 2003a: Dynamical predictability of intraseasonal variability associated with the Asian summer monsoon. *Quart. J. Roy. Meteor. Soc.,* **129,** 2897–2925.

——, and Coauthors, 2003b: AGCM simulations of intraseasonal variability associated with the Asian summer monsoon. *Climate Dyn.,* **21,** 423–446.

Wang, B., and LinHo, 2002: Rainy seasons of the Asian–Pacific summer monsoon. *J. Climate,* **15,** 386–398.

——, P. J. Webster, and H. Teng, 2005: Antecedents and self-induction of active-break south Asian monsoon unraveled by satellites. *Geophys. Res. Lett.,* **32,** L04704, doi:10.1029/2004GL020996.

Webster, P. J., 1983: Mechanisms of monsoon low-frequency variability: Surface hydrological effects. *J. Atmos. Sci.,* **40,** 2110–2124.

——, and S. Yang, 1992: Monsoon and ENSO: Selectively interactive systems. *Quart. J. Roy. Meteor. Soc.,* **118,** 877–926.

——, and C. Hoyos, 2004: Prediction of monsoon rainfall and river discharge on 15–30-day time scales. *Bull. Amer. Meteor. Soc.,* **85,** 1745–1765.

——, T. Palmer, M. Yanai, R. Tomas, V. Magaña, J. Shukla, and A. Yasunari, 1998: Monsoons: Processes, predictability and the prospects for prediction. *J. Geophys. Res.,* **103,** 14 451–14 510.

——, A. Moore, J. Loschnigg, and M. Leban, 1999: Coupled ocean–atmosphere dynamics in the Indian Ocean during 1997–98. *Nature,* **401,** 356–360.

Wentz, F. J., 1997: A well-calibrated ocean algorithm for Special Sensor Microwave/Imager. *J. Geophys. Res.,* **102,** 8703–8718.

——, and M. Schabel, 2000: Precise climate monitoring using complementary satellite data sets. *Nature,* **403,** 414–416.

Xie, S.-P., H. Xu, N. H. Saji, Y. Wang, and W. T. Liu, 2006: Role of narrow mountains in large-scale organization of Asian monsoon convection. *J. Climate,* **19,** 3420–3429.

Yasunari, T., 1979: Cloudiness fluctuations associated with the Northern Hemisphere summer monsoon. *J. Meteor. Soc. Japan,* **57,** 227–242.

——, 1981: Structure of an Indian summer monsoon system with around 40-day period. *J. Meteor. Soc. Japan,* **59,** 336–354.

Zuidema, P., 2003: Convective clouds over the Bay of Bengal. *Mon. Wea. Rev.,* **131,** 780–798.